Supplementary Information

Superlubricity via layered solidification and molecular reconfiguration of nanoconfined liquids

Bao Jin[1,2,3,10]*, Naizhou Du[4,10], He Zhang[5,6,10], Yuxuan Liu[7], Yutong Xiong[8], Yuwei Cao[1,2], Shuchun Huang[1,2], Jiaojiao Li[1,2], Wei-Tao Liu[7], Qingdao Zeng[8], Xiaohui Yu[5], Chenhui Zhang[1,2], Xiaowei Li[4,9]*, Yongyong He[1,2]*, Mohand O. Saed[3], Eugene M. Terentjev[3], Jianbin Luo[1,2]*

[1] *State Key Laboratory of Tribology in Advanced Equipment, Tsinghua University, Beijing, 100084, China*

[2] *Department of Mechanical Engineering, Tsinghua University, Beijing, 100084, China*

[3] *Cavendish Laboratory, University of Cambridge, Cambridge, CB3 0HE, UK*

[4] *School of Materials Science and Physics, China University of Mining and Technology, Xuzhou, 221116, China*

[5] *Beijing National Laboratory for Condensed Matter Physics and Institute of Physics, Chinese Academy of Sciences, Beijing, 100190, China*

[6] *School of Physical Sciences, University of Chinese Academy of Sciences, Beijing, 100049, China*

[7] *State Key Laboratory of Surface Physics, Key Laboratory of Micro and Nano Photonic Structures (MOE), and Department of Physics, Fudan University, Shanghai, 200433, China*

[8] *CAS Key Laboratory of Standardization and Measurement for Nanotechnology, CAS Center for Excellence in Nanoscience, National Center for Nanoscience and Technology (NCNST), Beijing, 100190, China*

[9] *Key Laboratory of Marine Materials and Related Technologies, Zhejiang Key Laboratory of Marine Materials and Protective Technologies, Ningbo Institute of Materials Technology and Engineering, Chinese Academy of Sciences, Ningbo, 315201, China*

[10] *These authors contributed equally*

*Corresponding author: heyy@mail.tsinghua.edu.cn (Yongyong He), lixw0826@gmail.com (Xiaowei Li), jinb@mail.tsinghua.edu.cn (Bao Jin), luojb@mail.tsinghua.edu.cn (Jianbin Luo)

Inventory of Supplementary Information

Supplementary Figures

atomic layer nanoconfinement.

Fig. S22 | Top-view snapshots of MD simulation models for 2-dodecanol, 3-dodecanol and 4-dodecanol systems at different simulation times.

Fig. S23 | Characteristic parameters obtained from MD simulations of alkanol molecules with hydroxyl functional groups located at different positions along the carbon backbone.

Other Supplementary Information for This Manuscript Include the Following:

Supplementary Movie 1 to 16

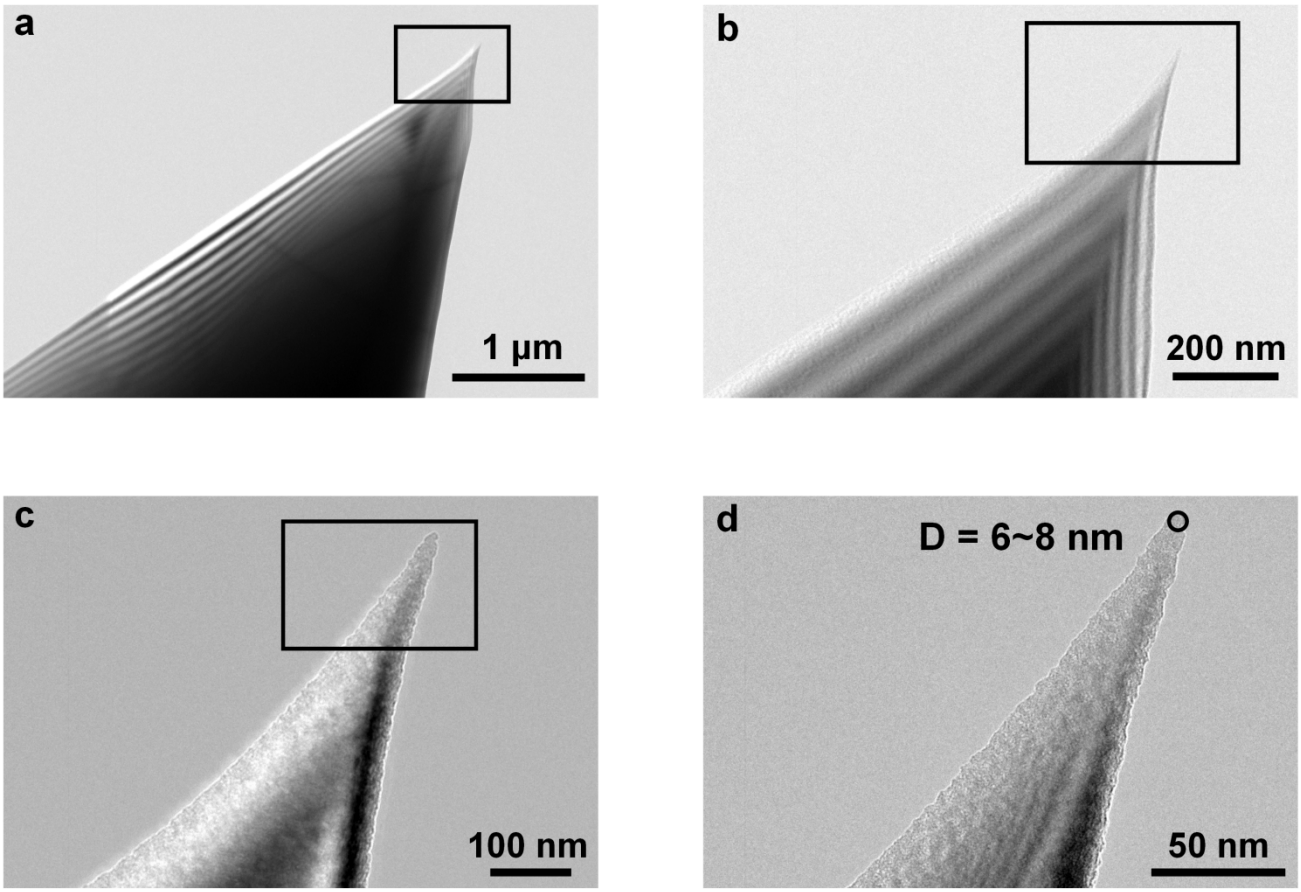

Fig. S1 | Morphology of a brand-new AFM tip. a Low-magnification image of the AFM tip. **b–d** Successively magnified views corresponding to the boxed regions in (**a**), (**b**), and (**c**), respectively.

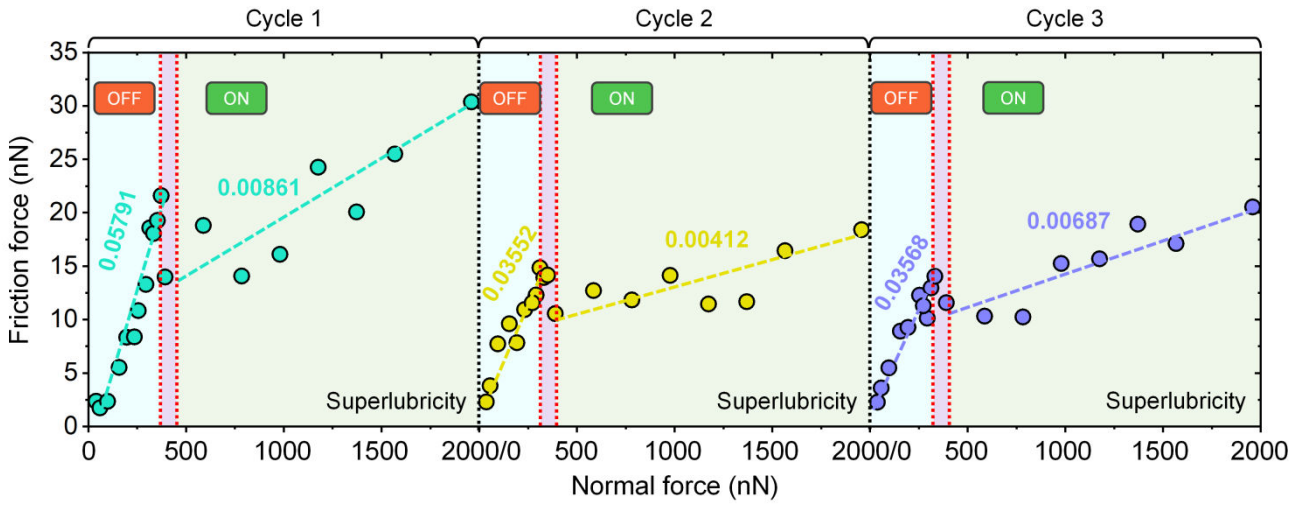

Fig. S2 | Switching effect of segmented superlubricity phenomenon. Friction behavior of 1-dodecanol within a graphene homogenenous junction over multiple cycles. The switching effect of the superlubricity phenomenon was captured, which is sensitive to variations in the normal force, corresponding to a sharp decrease in the COF within each cycle. The AFM tip sliding velocity was 4 μm/s for all three cycles. All AFM experiments were conducted at 26 ± 0.5°C.

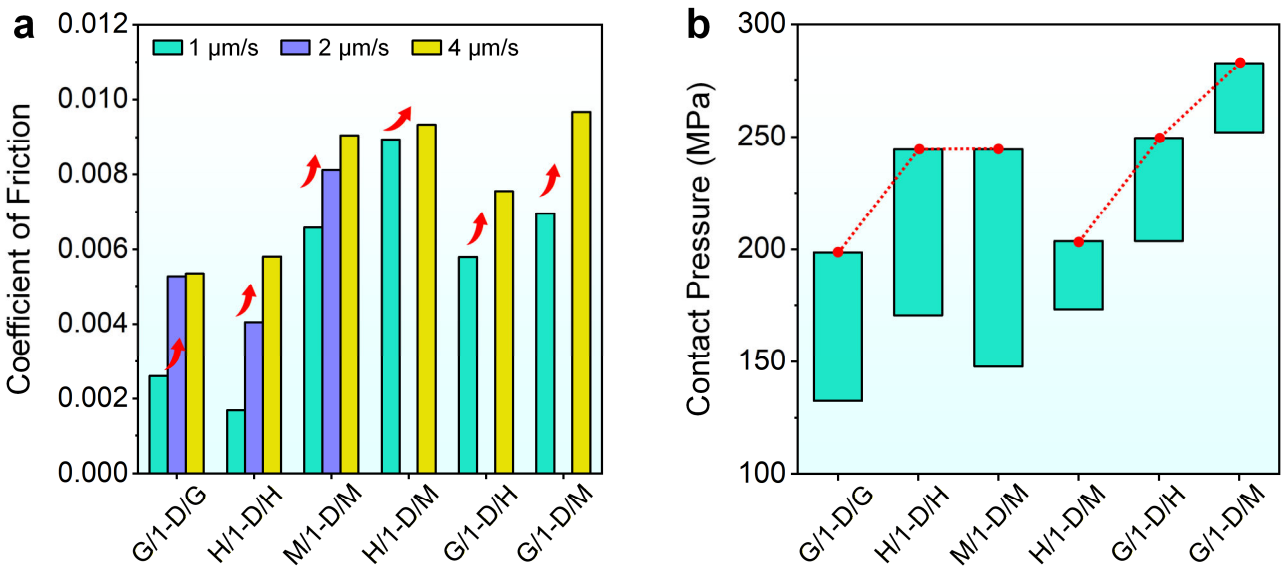

Fig. S3 | COF after phase transition (stage III) and contact pressure ranges of phase transition for 1-dodecanol under different nanoconfined geometries. a COF of the 1-dodecanol molecular layer after phase transition in homogeneous and heterogeneous junctions constructed from graphene, hBN, and MoS_2. The COF of 1-dodecanol after the phase transition increased with increasing of sliding velocity. **b** Contact pressure ranges corresponding to the phase transition of 1-dodecanol in the homogeneous and heterogeneous junctions constructed from different 2D materials.

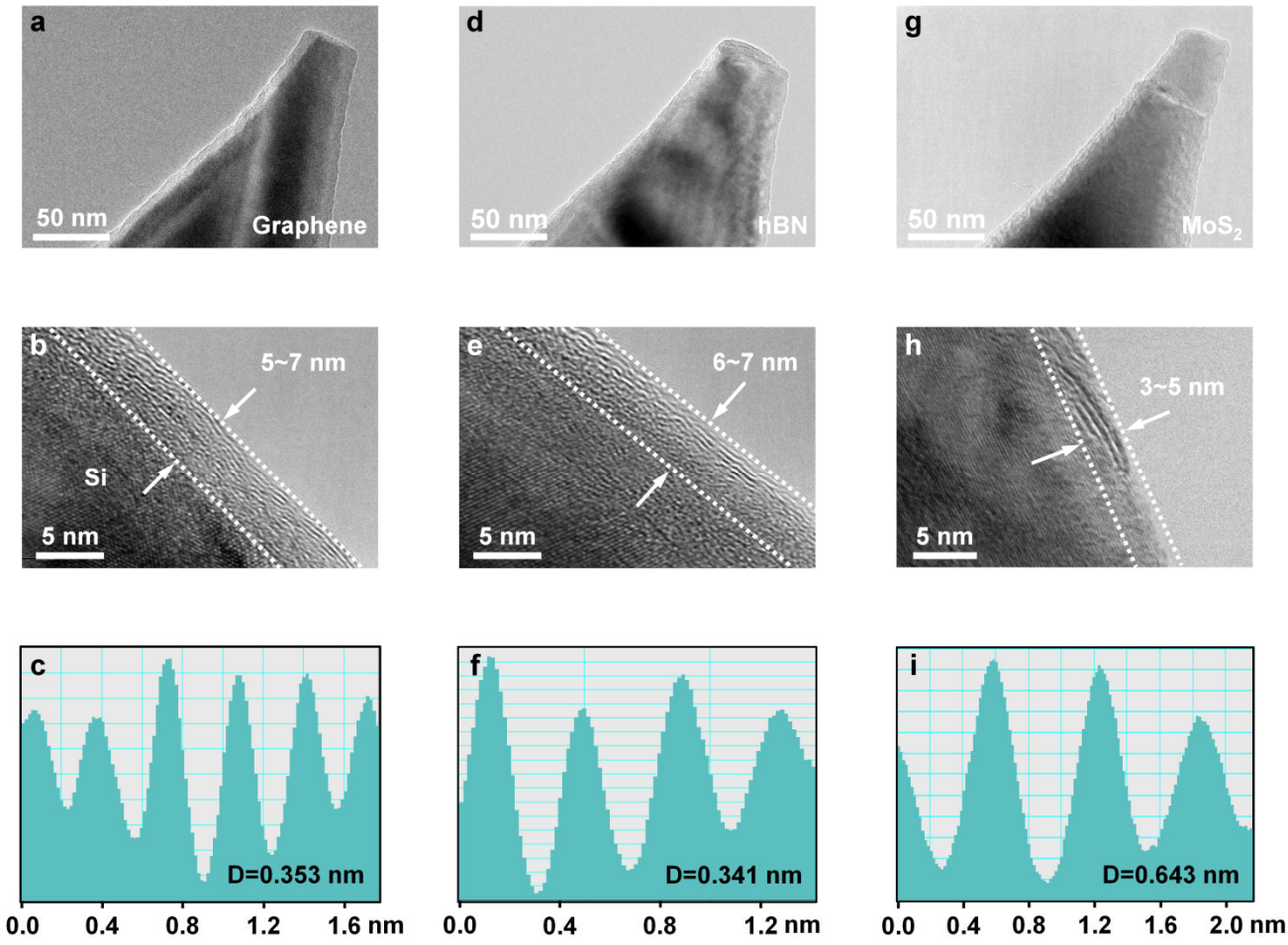

Fig. S4 | Morphology of AFM tips after friction experiments. a Morphology of an AFM tip coated with graphene atomic layers after friction experiments. **b** Morphology of graphene atomic layers formed on the surface of the AFM tip after friction experiments. **c** Lattice fringe spacing of the graphene atomic layers corresponding to (**b**). **d** Morphology of an AFM tip coated with hBN atomic layers after friction experiments. **e** Morphology of hBN atomic layers formed on the surface of the AFM tip after friction experiments. **f** Lattice fringe spacing of hBN atomic layers corresponding to (**e**). **g** Morphology of an AFM tip coated with MoS_2 atomic layers after friction experiments. **h** Morphology of MoS_2 atomic layers formed on the surface of the AFM tip after friction experiments. **i** Lattice fringe spacing of MoS_2 atomic layers corresponding to (**h**).

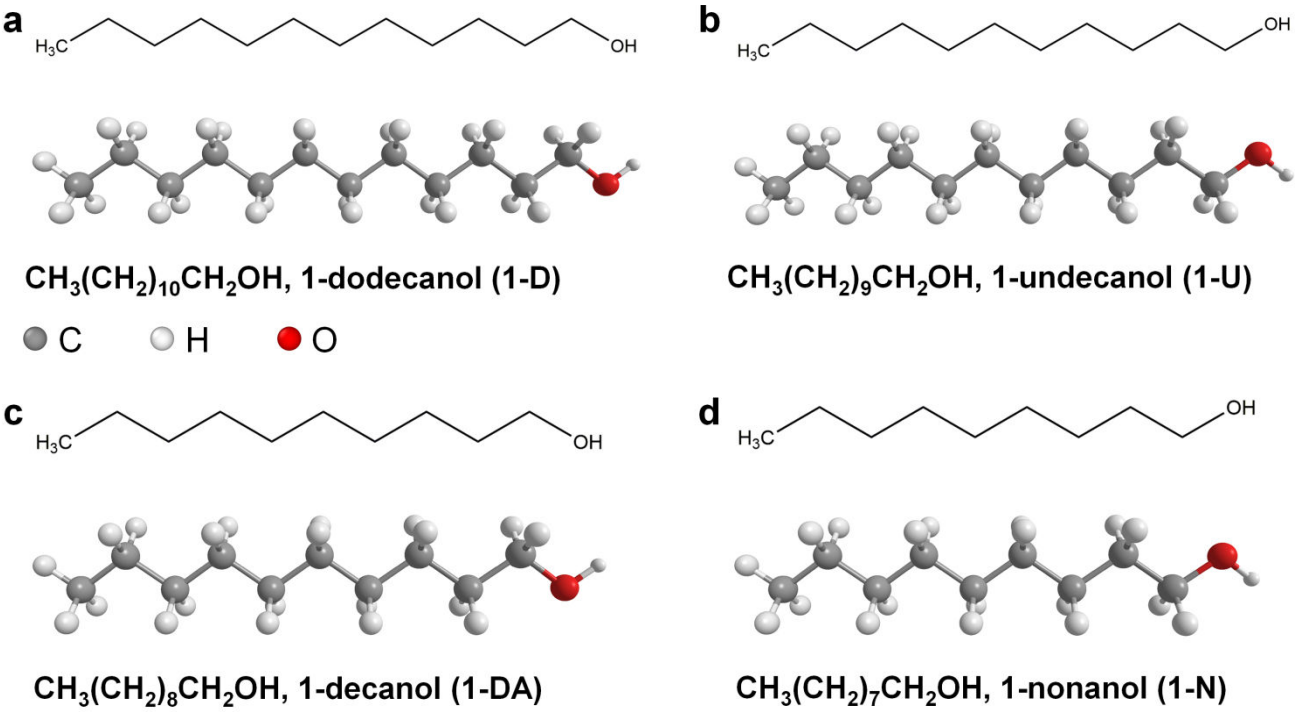

Fig. S5 | Ball-and-stick models and molecular structures of alkanols with different carbon chain lengths. a 1-dodecanol (1-D). **b** 1-undecanol (1-U). **c** 1-decanol (1-DA). **d** 1-nonanol (1-N). From 1-dodecanol to 1-nonanol, the number of carbon atoms in the molecular backbone decreased from 12 to 9.

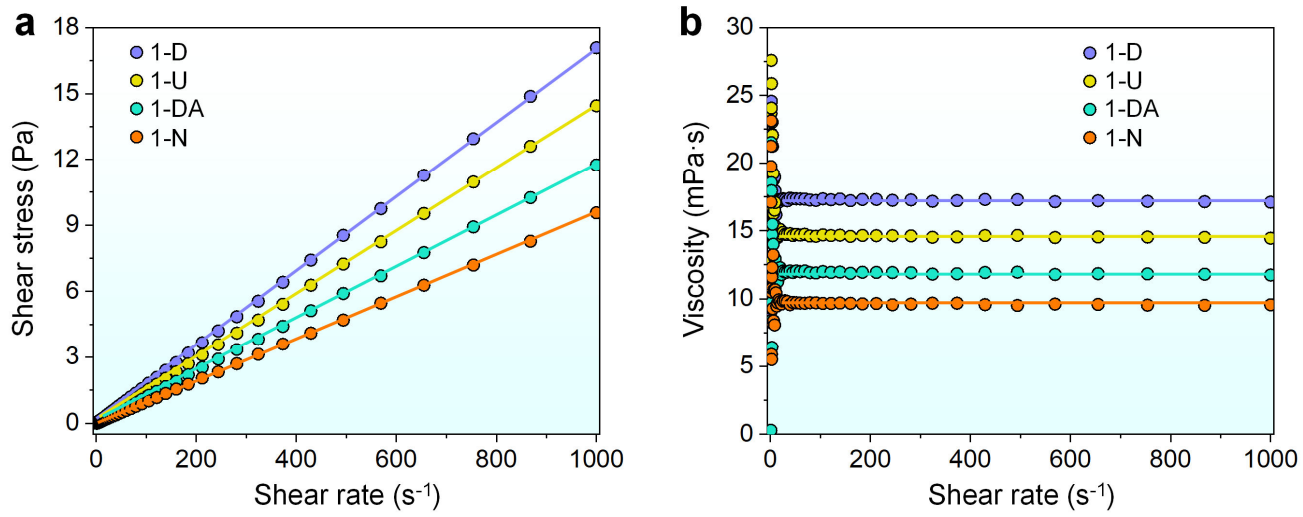

Fig. S6 | Viscosity–shear characteristics of alkanol molecules with different carbon chain lengths. a Relationship between shear stress (τ) and shear rate (γ) for alkanols. The shear stress τ exhibits a linear dependence on shear rate γ. **b** Relationship between viscosity (η) and shear rate (γ) for alkanols. Viscosity η is independent of shear rate γ. The viscosities of 1-D, 1-U, 1-DA, and 1-N are 17.3, 14.6, 11.9, and 9.6 mPa·s, respectively. Alkanols with different carbon chain lengths exhibit typical Newtonian fluid behavior, for which the relationship between shear stress τ, shear rate γ, and viscosity η is given by $\tau = \eta\gamma$. All experiments were conducted at 30°C.

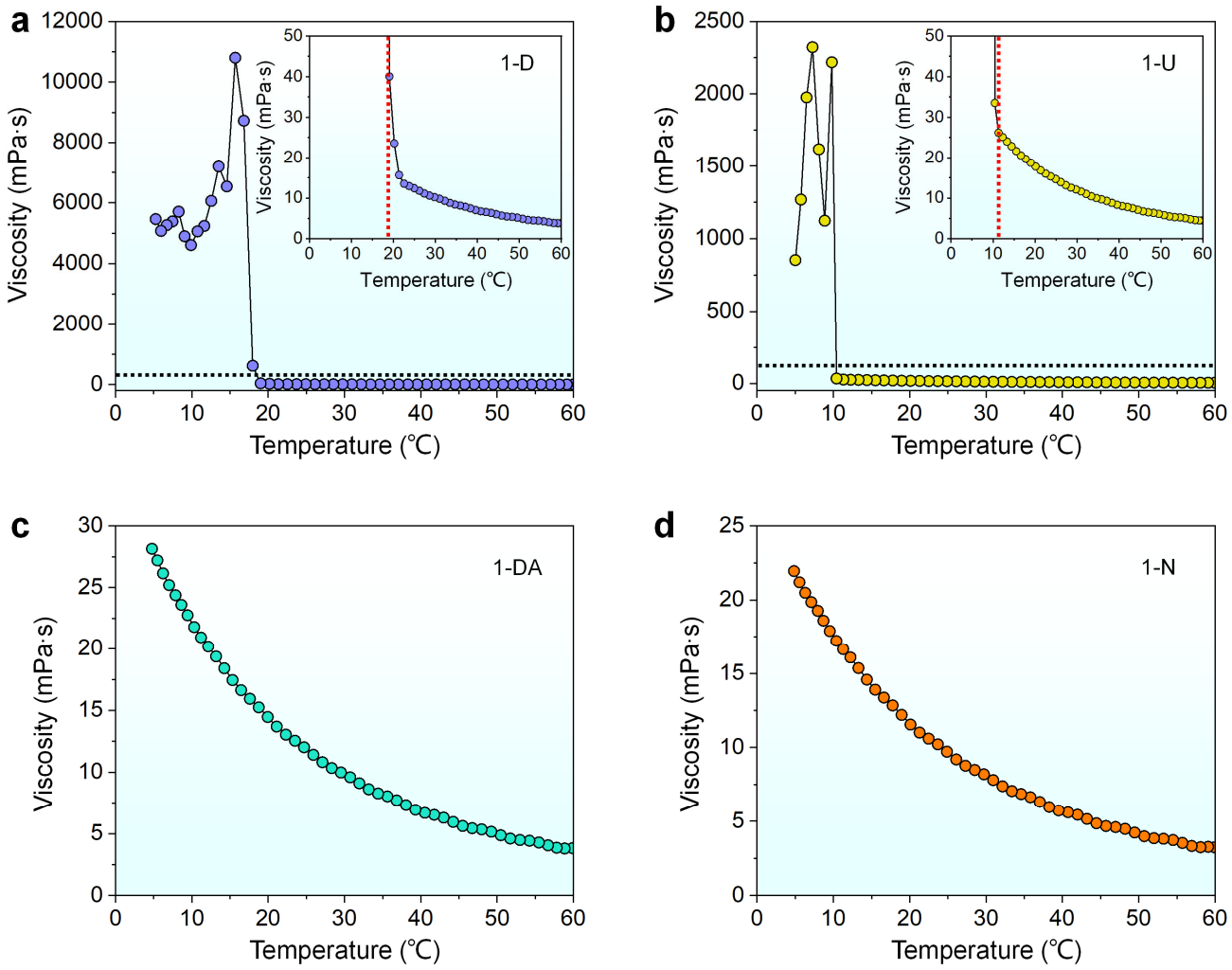

Fig. S7 | Viscosity–temperature characteristics of alkanol molecules with different carbon chain lengths. a Viscosity–temperature behavior of 1-D. When the temperature decreased to approximately 18.5°C, a sudden increase and fluctuation in viscosity were observed, arising from the liquid–solid phase transition. **b** Viscosity–temperature behavior of 1-U. The liquid–solid phase transition led to a sharp increase in viscosity when the temperature decreased to approximately 11°C. **c** Viscosity–temperature behavior of 1-DA. **d** Viscosity–temperature behavior of 1-N. For all measurements, the shear rate was fixed at 500 s^{-1}.

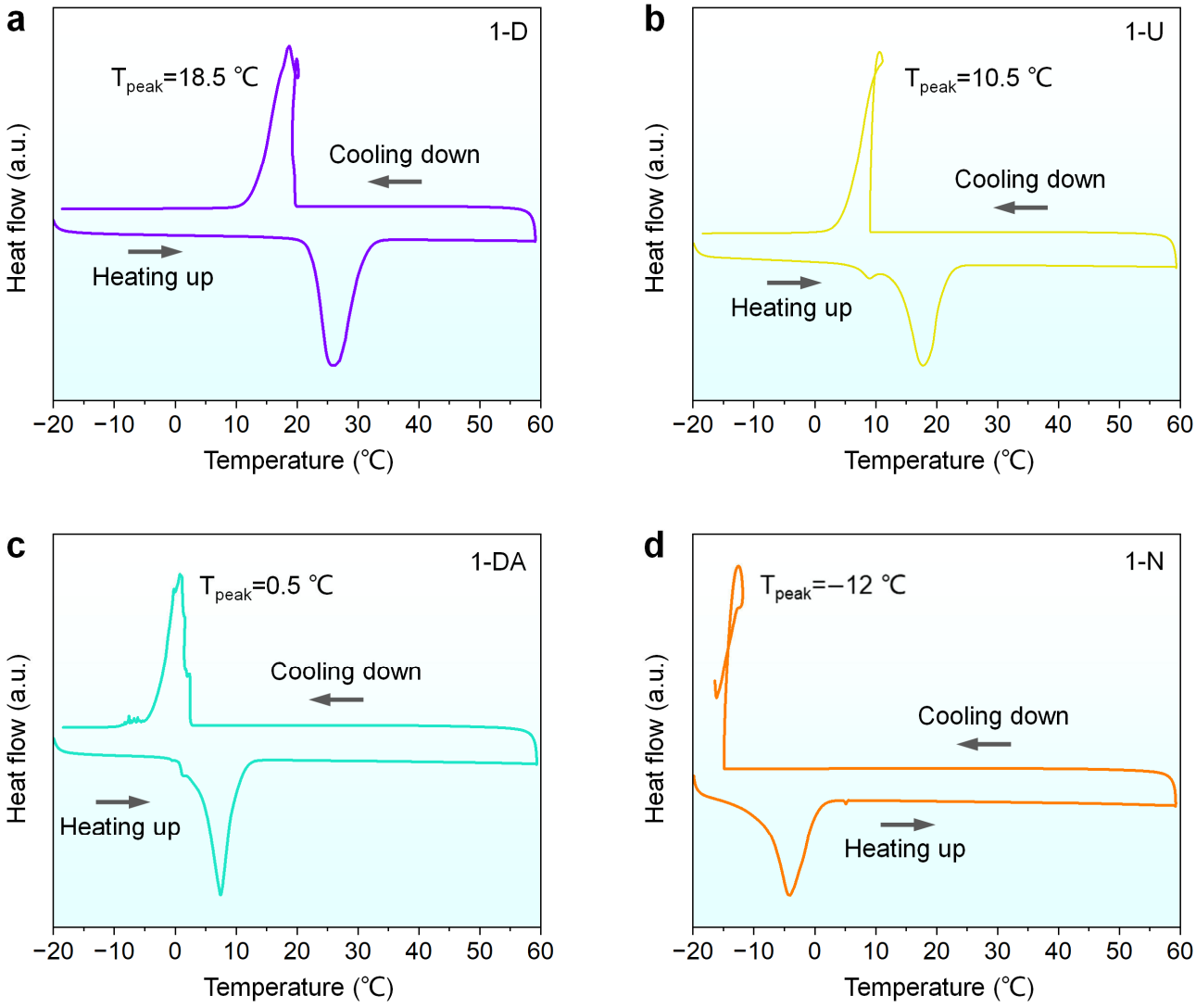

Fig. S8 | Differential scanning calorimetry (DSC) curves of alkanol molecules with different carbon chain lengths. a DSC curve of 1-D. **b** DSC curve of 1-U. **c** DSC curve of 1-DA. **d** DSC curve of 1-N. The temperature ramp rate during both heating and cooling was 5 °C/min. The freezing points of 1-D, 1-U, 1-DA, and 1-N are 18.5, 10.5, 0.5, and −12°C, respectively.

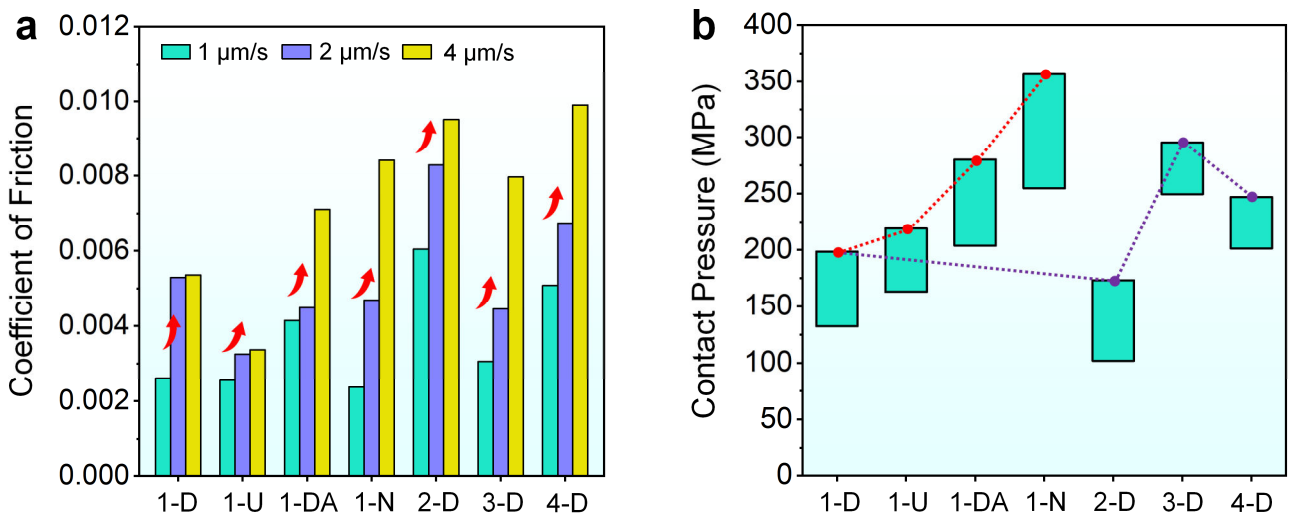

Fig. S9 | COF after phase transition and contact pressure ranges associated with phase transitions for different alkanol molecular layers in a graphene homogeneous junction. a COF of different nanoconfined alkanol molecular layers after phase transition. In general, the COF of alkanols after phase transition increases with increasing sliding velocity. Owing to relaxation effects of alkanol molecules during the phase transition under nanoconfinement, the occurrence of phase transition becomes less favorable at high sliding velocities. **b** Contact pressure ranges corresponding to the phase transitions of different nanoconfined alkanol molecular layers.

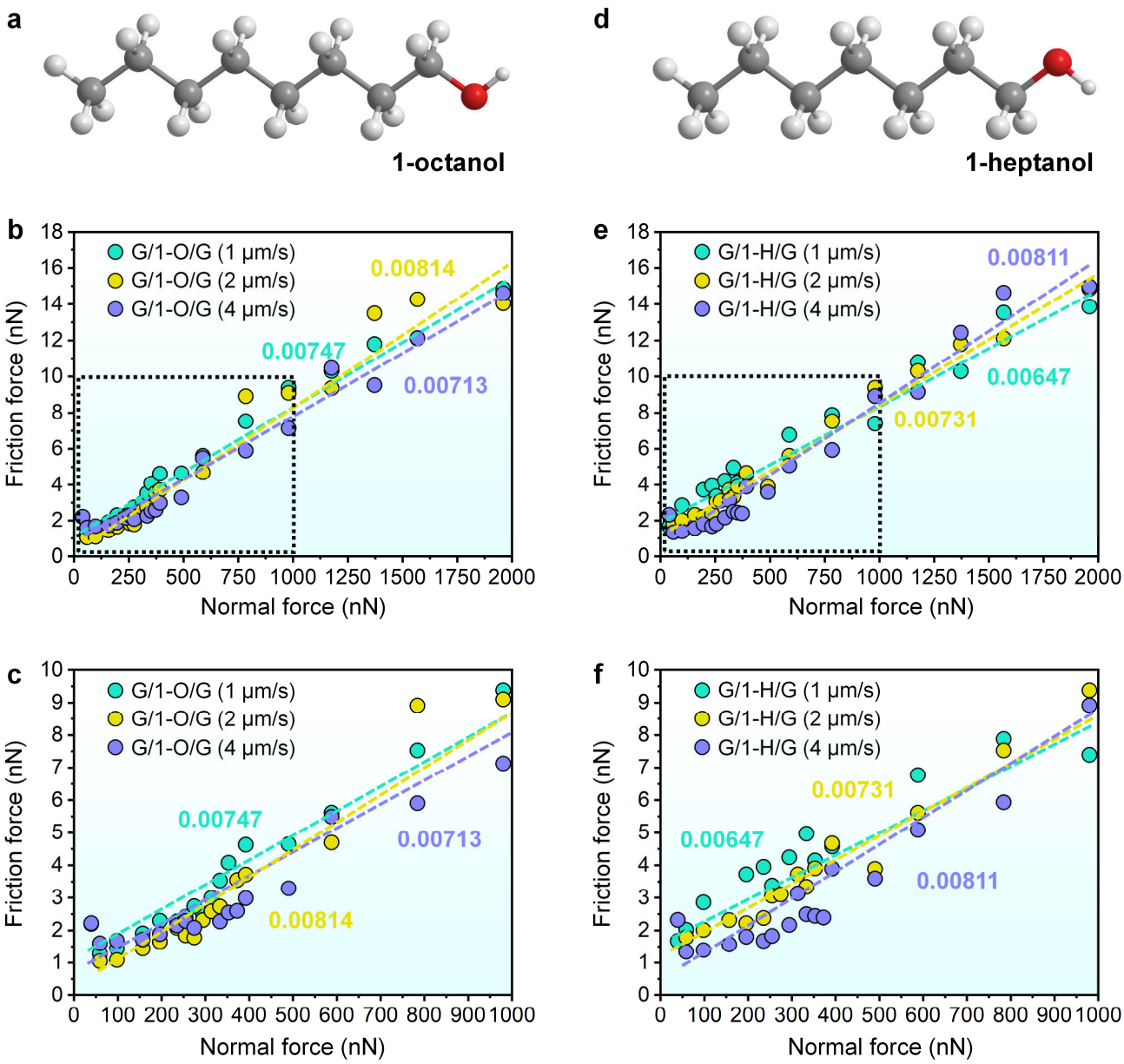

Fig. S10 | Friction behavior of 1-octanol and 1-heptanol molecular layers within the nanoconfined geometry formed by graphene atomic layers. a Molecular structure of 1-octanol. **b** Friction behavior of 1-octanol in a homogeneous graphene junction. G/1-O/G represents the friction data of 1-octanol within the nanoconfined interface formed between a graphene-coated AFM tip and a HOPG substrate. All colored numbers represent the COF obtained by fitting the friction data of the same color. **c** Enlarged view of the black dashed box region in (**b**). There are no significant segmented features in the COF of 1-octanol. **d** Molecular structure of 1-heptanol. **e** Friction behavior of 1-heptanol in a homogeneous graphene junction. G/1-H/G represents the friction data of 1-heptanol within the nanoconfined interface formed between a graphene-coated AFM tip and a HOPG substrate. **f** Enlarged view of the black dashed box region in (**e**). There are no significant segmented features in the COF of 1-heptanol. Neither 1-octanol nor 1-heptanol exhibits segmental superlubricity in nanoconfined geometries. All AFM experiments were conducted at 26 ± 0.5°C.

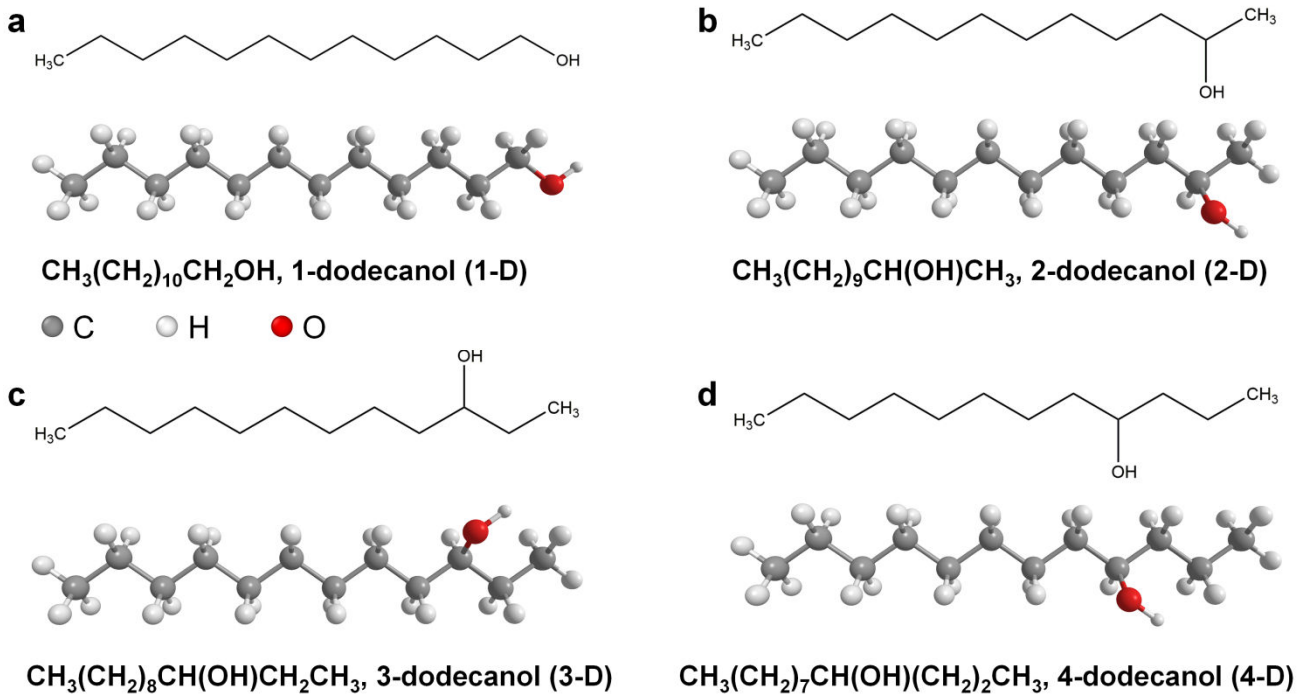

Fig. S11 | Ball-and-stick models and molecular structures of alkanols with hydroxyl functional groups located at different positions along the carbon backbone. a 1-dodecanol (1-D). **b** 2-dodecanol (2-D). **c** 3-dodecanol (3-D). **d** 4-dodecanol (4-D). All alkanols share the same 12-carbon backbone, whereas the hydroxyl group is bonded to the carbon atom at positions 1, 2, 3, and 4, respectively.

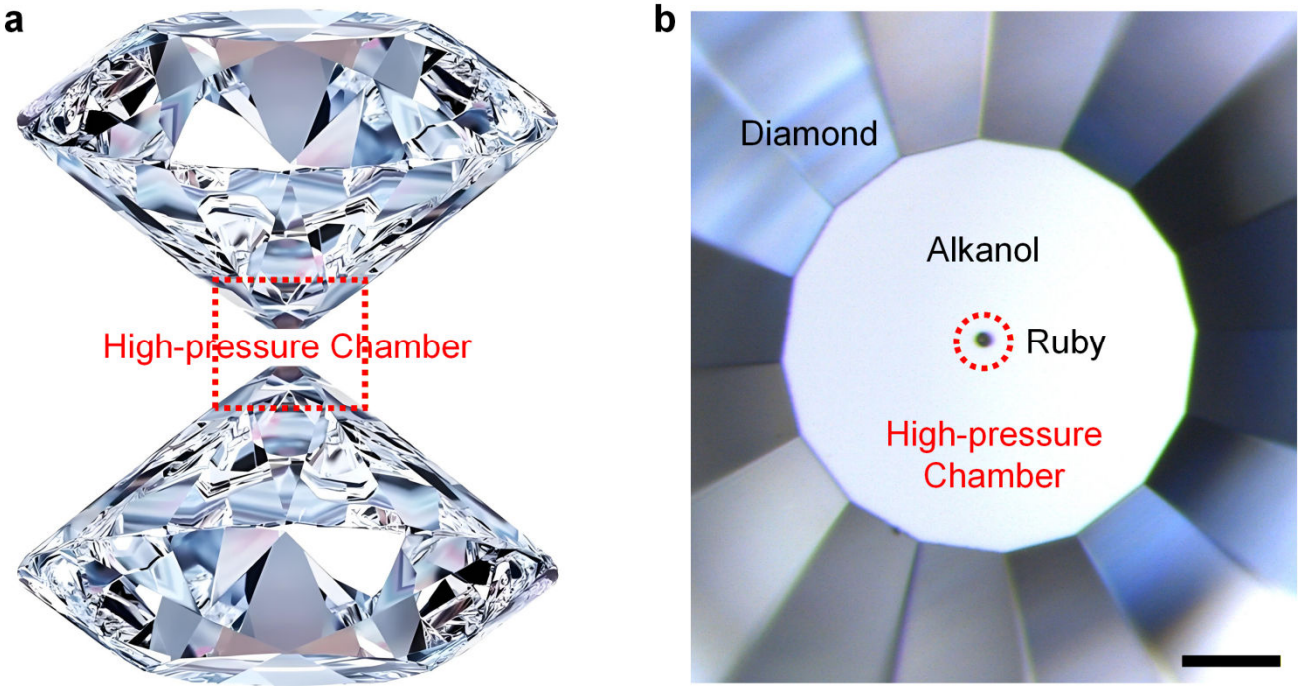

Fig. S12 | Diamond anvil cell (DAC) equipment. a Schematic illustration of DAC. Two flat-ground diamond culets were arranged face-to-face to form a high-pressure chamber. The pressure inside the chamber was controlled using four uniformly distributed screws. **b** Top view of high-pressure cell. The alkanol liquid to be tested completely filled the chamber. A ruby microsphere with a diameter of 5–10 μm was preloaded into the chamber. The pressure inside the high-pressure cell was calibrated in real time by monitoring the pressure-induced shift in the ruby fluorescence spectrum. Scale bar, 100 μm.

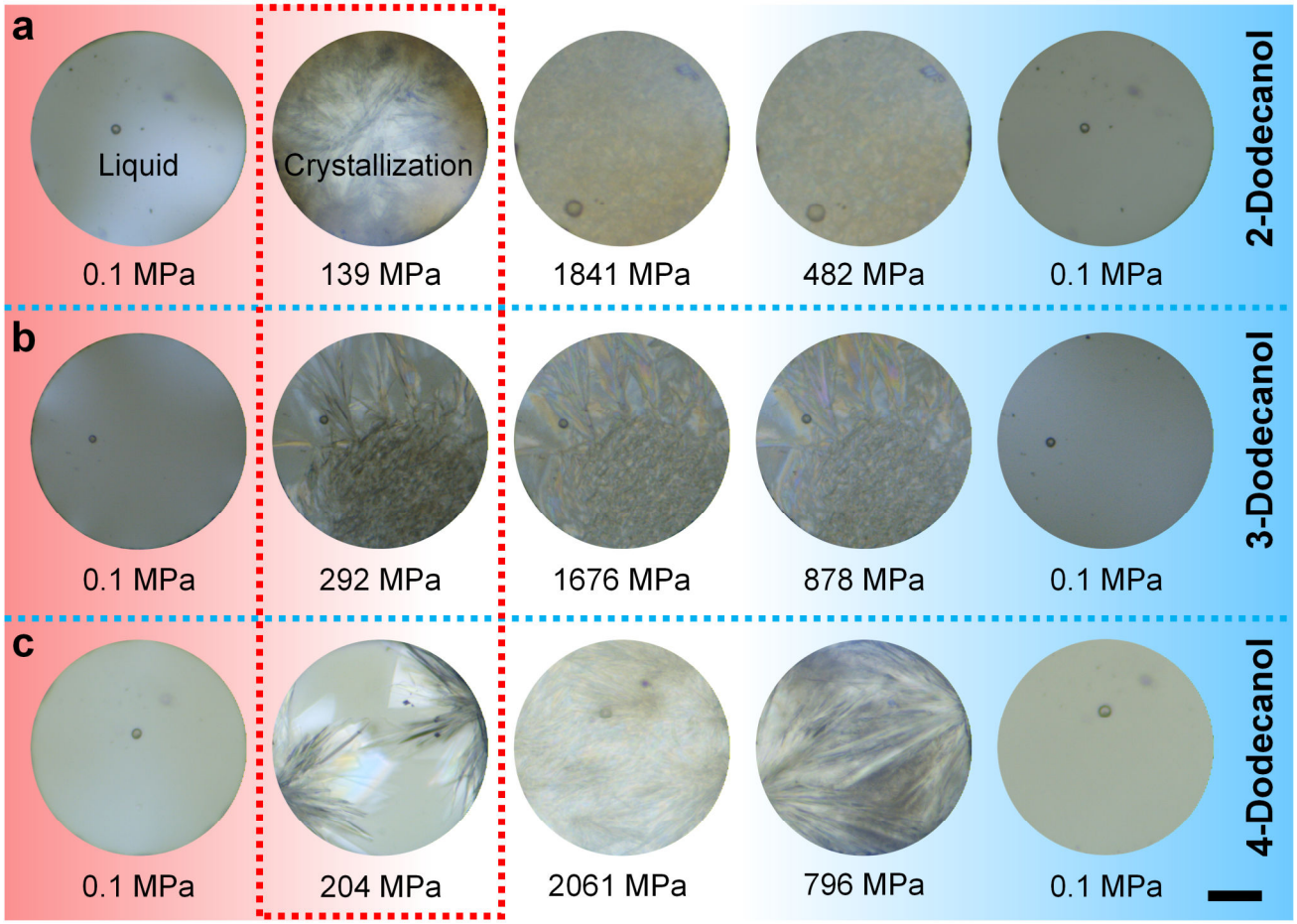

Fig. S13 | Pressure-induced reversible phase transitions of alkanol liquids with hydroxyl groups located at different positions along the carbon backbone. a 2-Dodecanol. The critical pressure for the phase transition of 2-dodecanol was 139 MPa. **b** 3-Dodecanol. The critical pressure for the phase transition of 3-dodecanol was 292 MPa. **c** 4-Dodecanol. The critical pressure for the phase transition of 4-dodecanol was 204 MPa. For all alkanols, the pressure-induced phase transition process was reversible, that is, the alkanol molecules reverted from the solid phase to the liquid phase upon decreasing the interfacial pressure. All experiments were conducted at 26 ± 0.5°C. Scale bar, 100 μm.

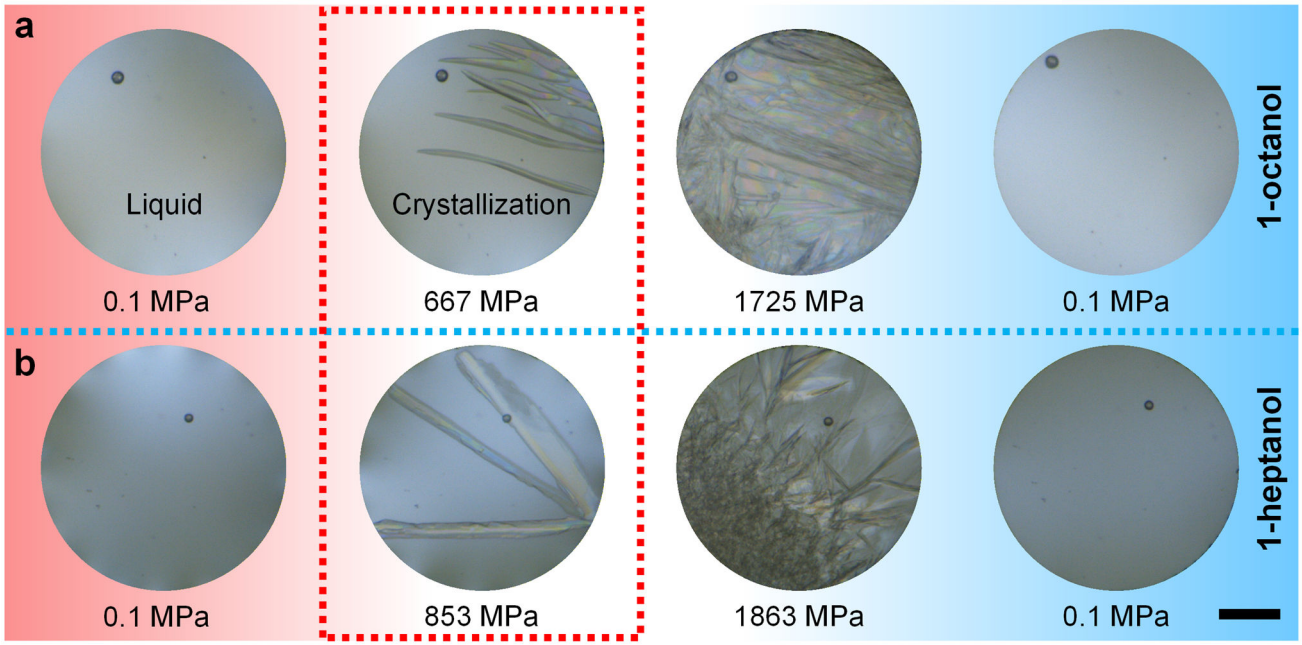

Fig. S14 | Pressure-induced phase transitions of alkanol liquid. a 1-Octanol. The critical pressure for the phase transition of 1-octanol was up to 667 MPa. **b** 1-Heptanol. The critical pressure for the phase transition of 1-heptanol was as high as 853 MPa. The critical pressure required for the phase transition of 1-dctanol and 1-octanol is prohibitively high, making it extremely difficult to stably achieve such demanding pressure conditions at the AFM tip contact region. As a result, the COFs of 1-dctanol and 1-octanol do not exhibit any significant segmented characteristics. All experiments were conducted at 26 ± 0.5°C. Scale bar, 100 μm.

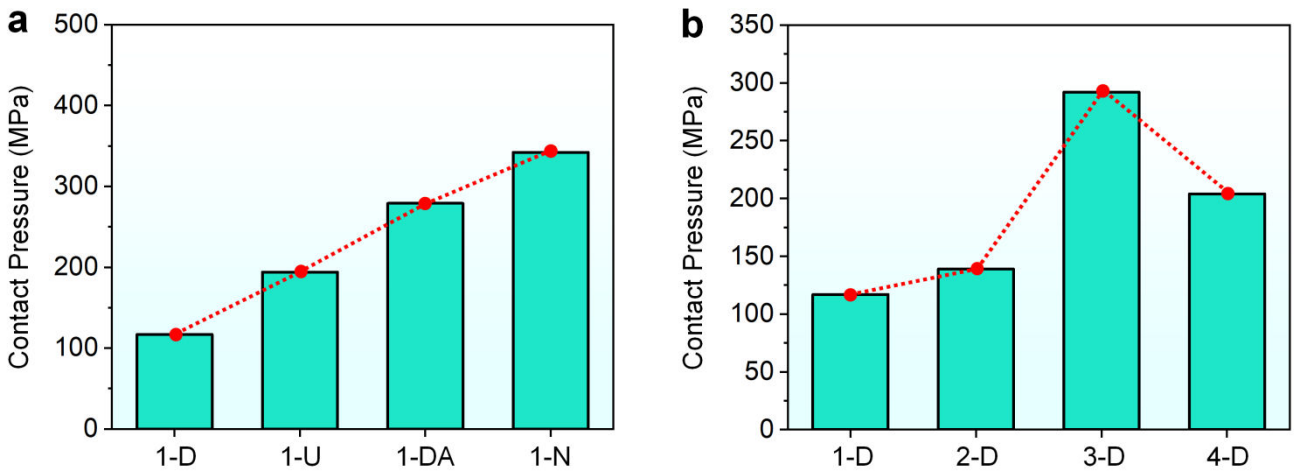

Fig. S15 | Critical contact pressures for liquid–solid phase transitions of different alkanol molecules determined by DAC experiments. a Alkanol molecules with different carbon chain lengths. As the carbon chain length decreased, the critical contact pressure required for the liquid–solid phase transition increased. **b** Alkanol molecules with hydroxyl functional groups bonded at different positions along the carbon backbone. In general, when the hydroxyl group is bonded closer to the center of the carbon backbone, a higher critical contact pressure is required for the phase transition of alkanol molecules (1-D, 2-D, and 3-D). However, 4-D represents an exception and does not follow this trend. All experiments were conducted at 26 ± 0.5°C.

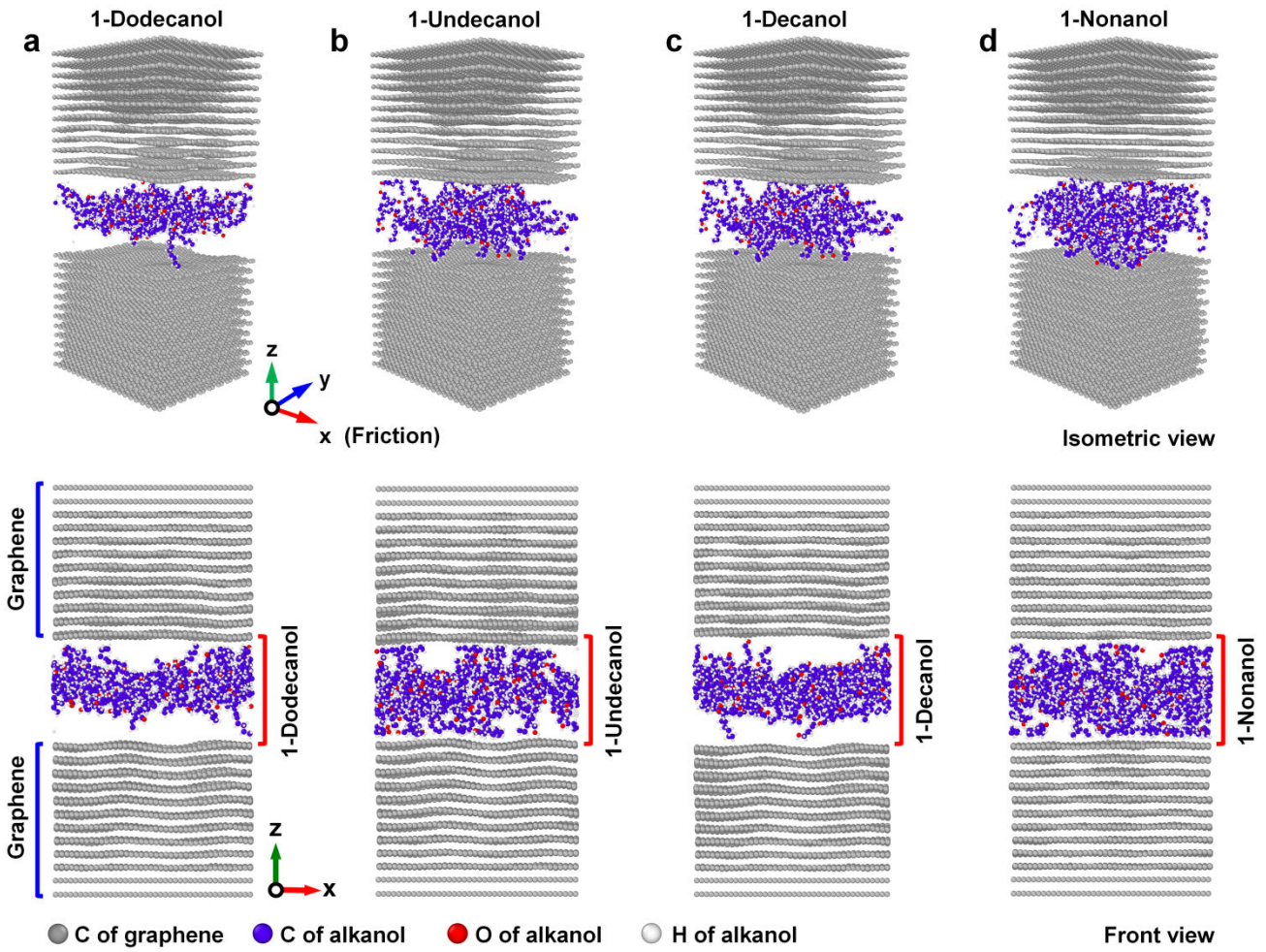

Fig. S16 | MD simulation models of alkanol molecules with different carbon chain lengths under 2D atomic layer nanoconfinement. Isometric and front views of the MD simulation model for 1-dodecanol (**a**), 1-undecanol (**b**), 1-decanol (**c**), and 1-nonanol (**d**) systems. Alkanol molecules are confined within a low-dimensional nanoconfined geometry formed by graphene atomic layers. The upper graphene layer was slid at a constant velocity of 1 m/s. Detailed simulation parameters are described in the Methods section.

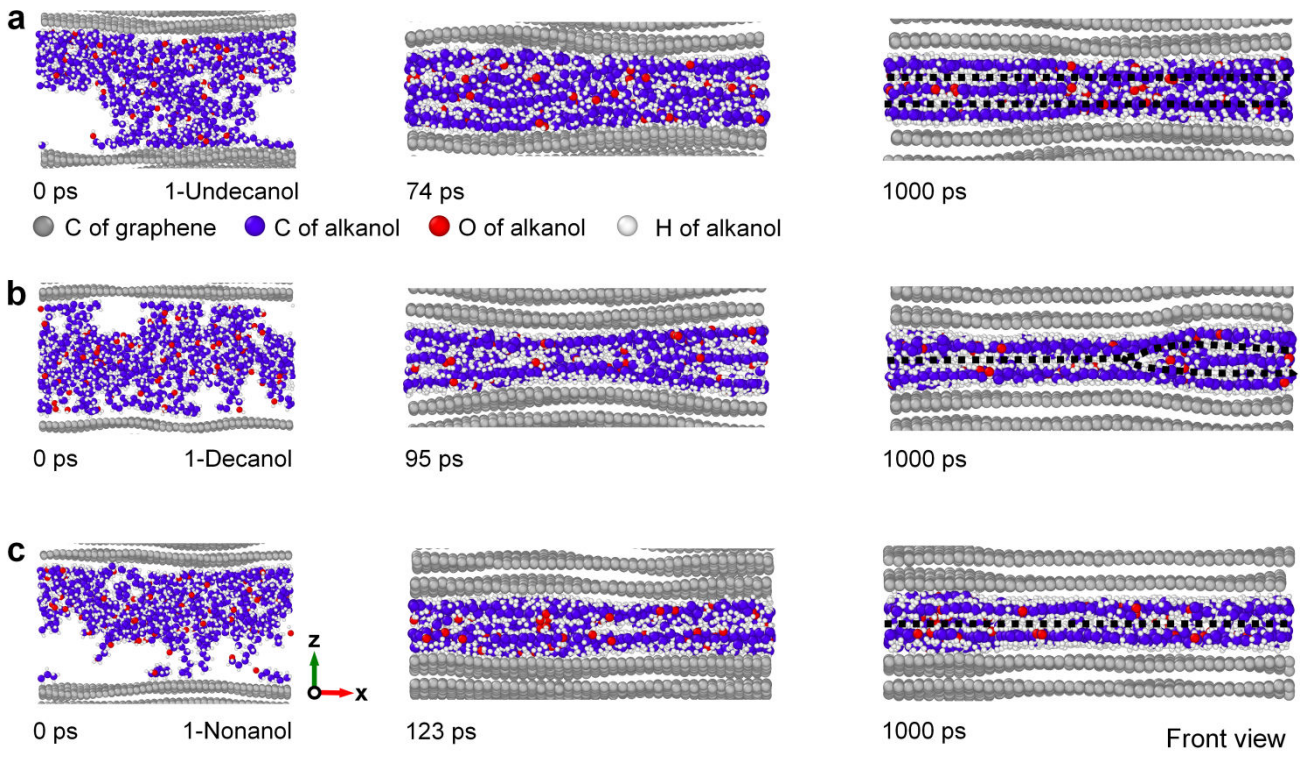

Fig. S17 | Front-view snapshots of MD simulation models of alkanol systems at different simulation times. a 1-Undecanol systems. **b** 1-Decanol systems. **c** 1-Nonanol systems. Before the sliding began, the relaxed alkanol molecules were randomly distributed within the nanoconfined geometry (0 ps in **a–c**). After sliding began, 1-undecanol, 1-decanol, and 1-nonanol molecules completed the migration and reconfiguration processes within approximately 74, 95, and 123 ps, respectively, corresponding to the occurrence of a phase transition. After completion of the phase transition, 1-undecanol molecules spontaneously self-assembled into a three-layer-ordered molecular structure, whereas 1-decanol and 1-nonanol molecules formed two-layer structures (1000 ps in **a–c**).

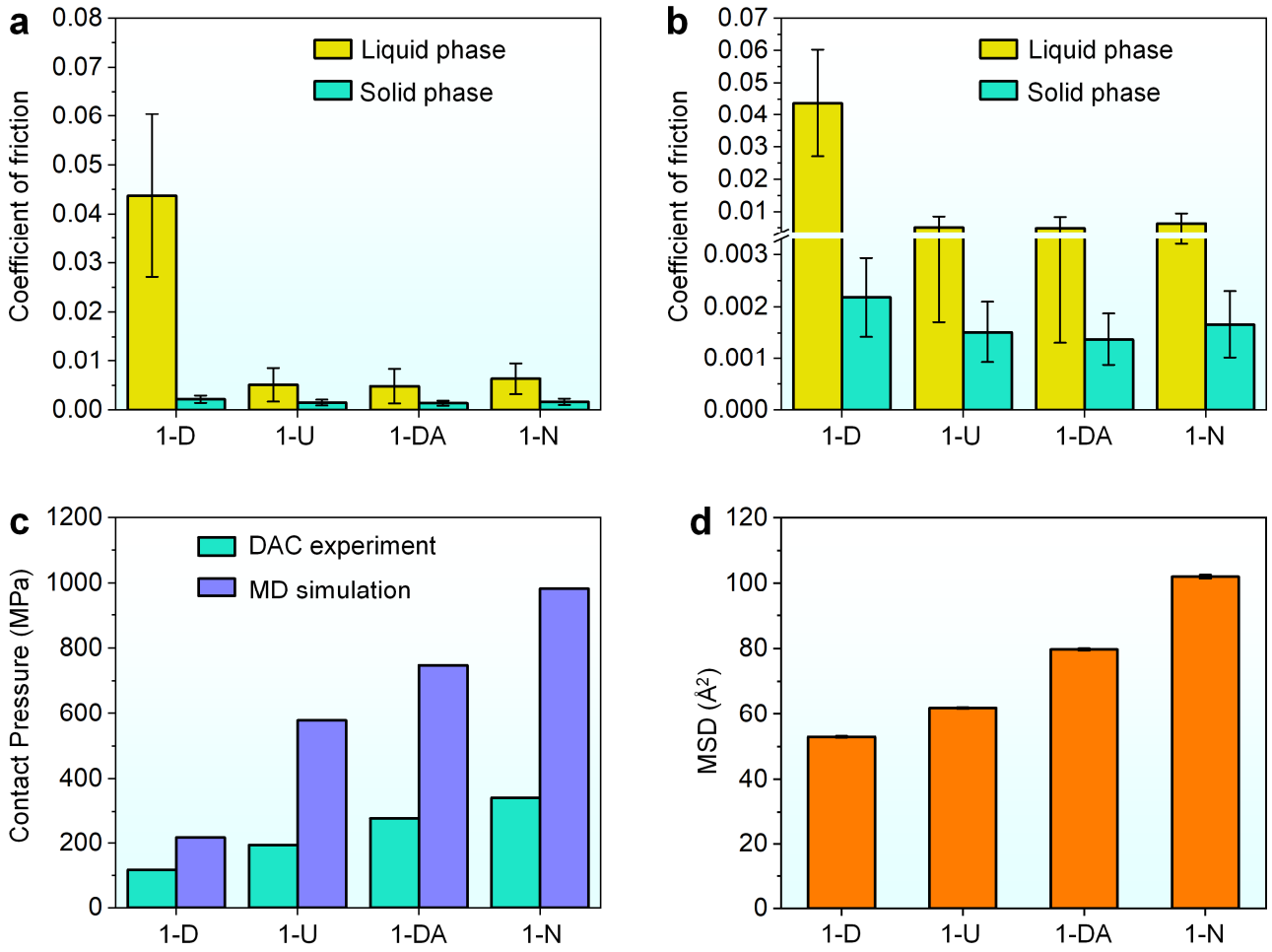

Fig. S18 | Characteristic parameters obtained from MD models of alkanol molecules. a Average COF of alkanol molecules in the liquid and solid phases. **b** Enlarged view of the average coefficients of friction shown in (**a**). The average COF in the liquid phase was calculated over the first 50 ps of the MD simulations, whereas the average COF in the solid phase was calculated over the final 400 ps of the simulations. After the phase transition of alkanol molecules under nanoconfinement, the COF decreased significantly. **c** Critical contact pressures for the phase transition of alkanol molecules obtained from DAC experiments and MD simulations. **d** Stable values of the MSD parameters of the alkanol molecules after phase transition. The data in (**d**) were obtained by averaging the values of the MSD parameters over the final 200 ps of the MD simulations. The stable values of the MSD parameters increased with decreasing carbon chain length of the alkanol molecules.

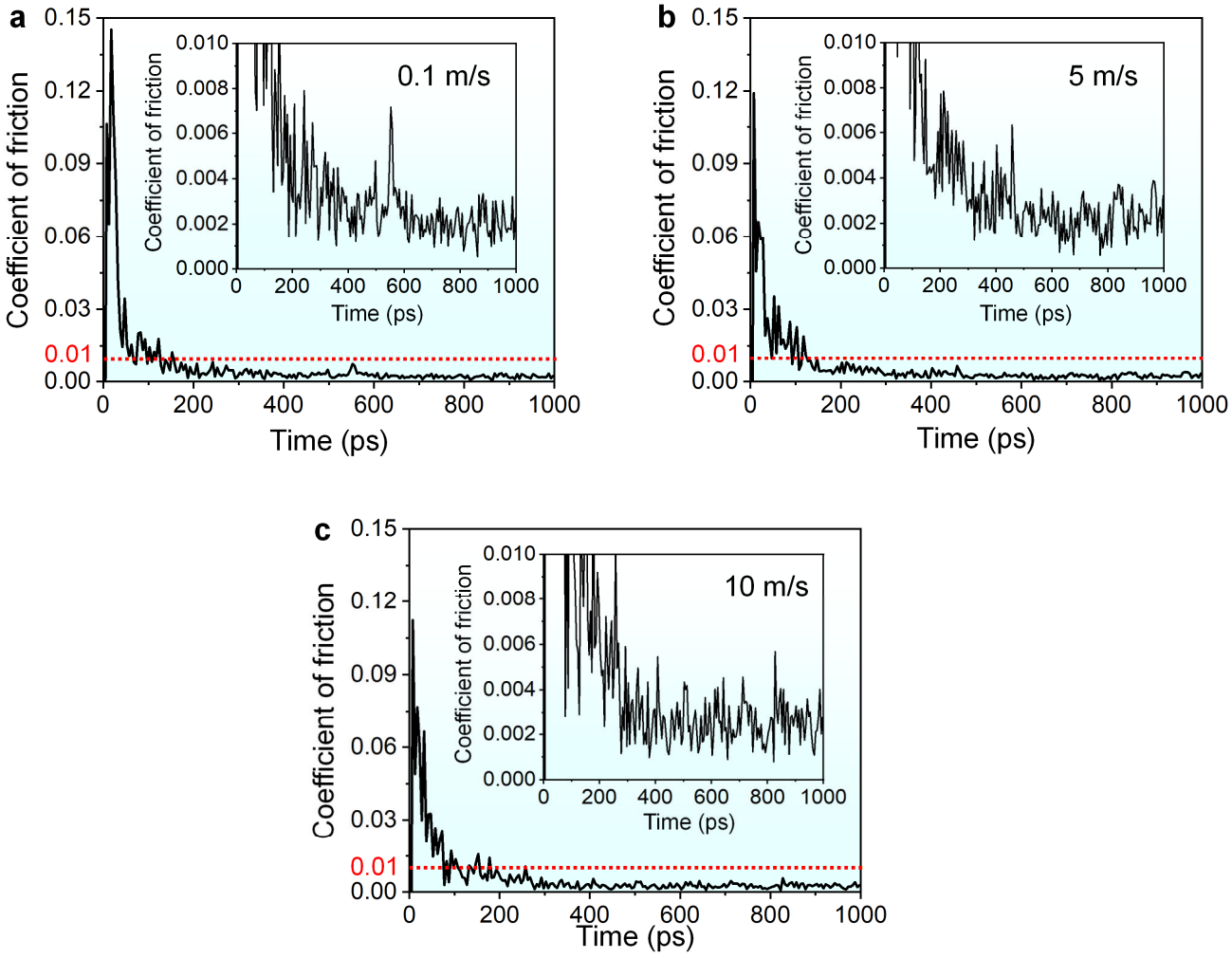

Fig. S19 | Time-dependent COF of MD simulation for 1-dodecanol at different sliding velocities. **a** 0.1 m/s. **b** 5 m/s. **c** 10 m/s. The inset is an enlarged view of the red dashed box.

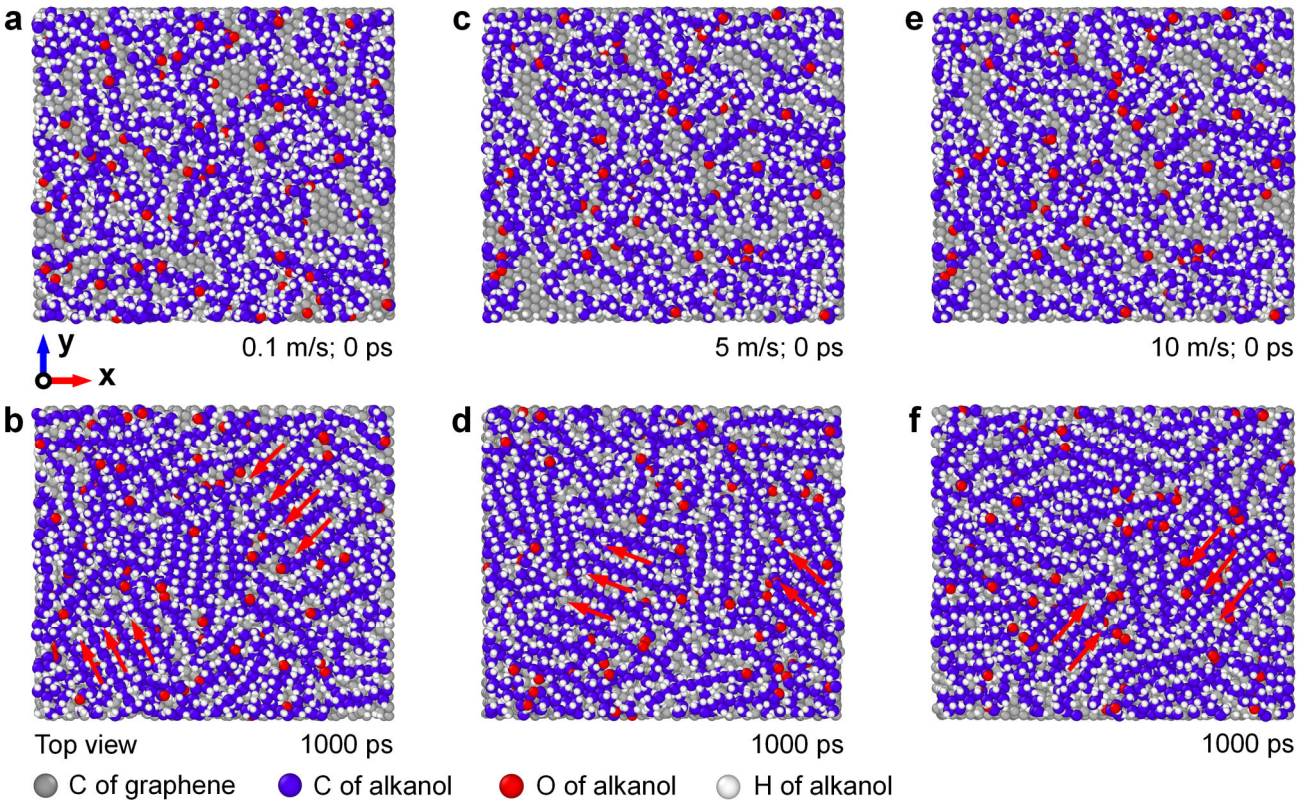

Fig. S20 | Top-view snapshots of MD simulation models for 1-dodecanol at different sliding velocities. a, b When the sliding velocity is 0.1 m/s, the molecular configurations of 1-dodecanol at 0 ps (**a**) and 1000 ps (**b**). **c, d** When the sliding velocity is 5 m/s, the molecular configurations of 1-dodecanol at 0 ps (**c**) and 1000 ps (**d**). **e, f** When the sliding velocity is 10 m/s, the molecular configurations of 1-dodecanol at 0 ps (**e**) and 1000 ps (**f**). After phase transition, 1-dodecanol forms a polycrystalline molecular configuration at different sliding velocities. In the top-view MD models, the upper graphene layers are hidden for clarity.

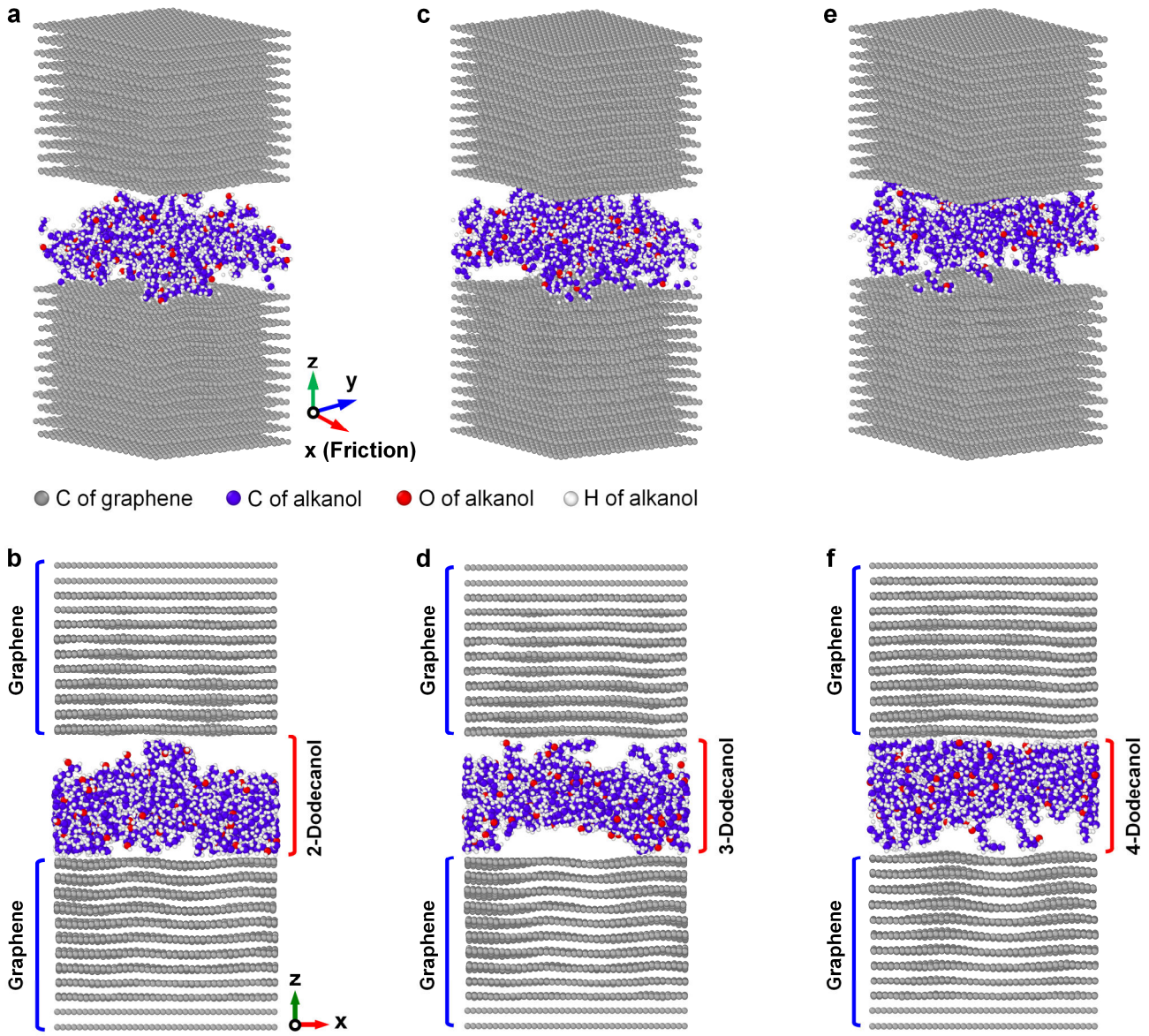

Fig. S21 | MD simulation models of 2-dodecanol, 3-dodecanol and 4-dodecanol molecules under 2D atomic layer nanoconfinement. a, b Isometric (**a**) and front (**b**) views of the MD simulation model of the 2-dodecanol system. **c, d** Isometric (**c**) and front (**d**) views of the MD simulation model of the 3-dodecanol system. **e, f** Isometric (**e**) and front (**f**) views of the MD simulation model of the 4-dodecanol system. The upper graphene layer was slid along the x-axis at a constant velocity of 1 m/s. Detailed MD simulation parameters are described in the Methods section.

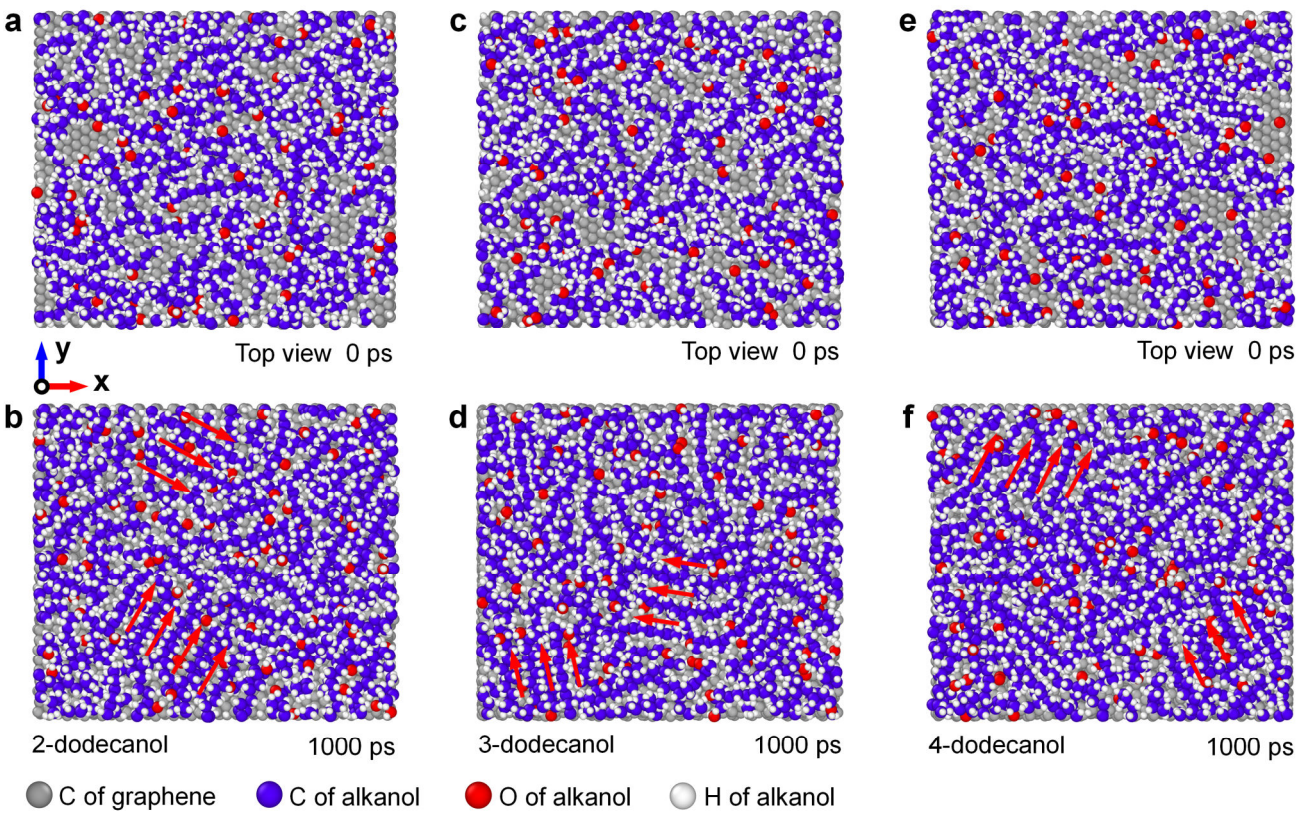

Fig. S22 | Top-view snapshots of MD simulation models for 2-dodecanol, 3-dodecanol and 4-dodecanol systems at different simulation times. a, b Molecular configurations of 2-dodecanol at 0 ps (**a**) and 1000 ps (**b**). **c, d** Molecular configurations of 3-dodecanol at 0 ps (**c**) and 1000 ps (**d**). **e, f** Molecular configurations of 4-dodecanol at 0 ps (**e**) and 1000 ps (**f**). At the beginning of the simulation (0 ps), 2-dodecanol, 3-dodecanol and 4-dodecanol molecules were randomly distributed in a disordered state. After the phase transition (1000 ps), the molecules exhibited a pronounced orientational order, and the molecular configurations adopted polycrystalline structures. In the top-view MD models, the upper graphene layers are hidden for clarity.

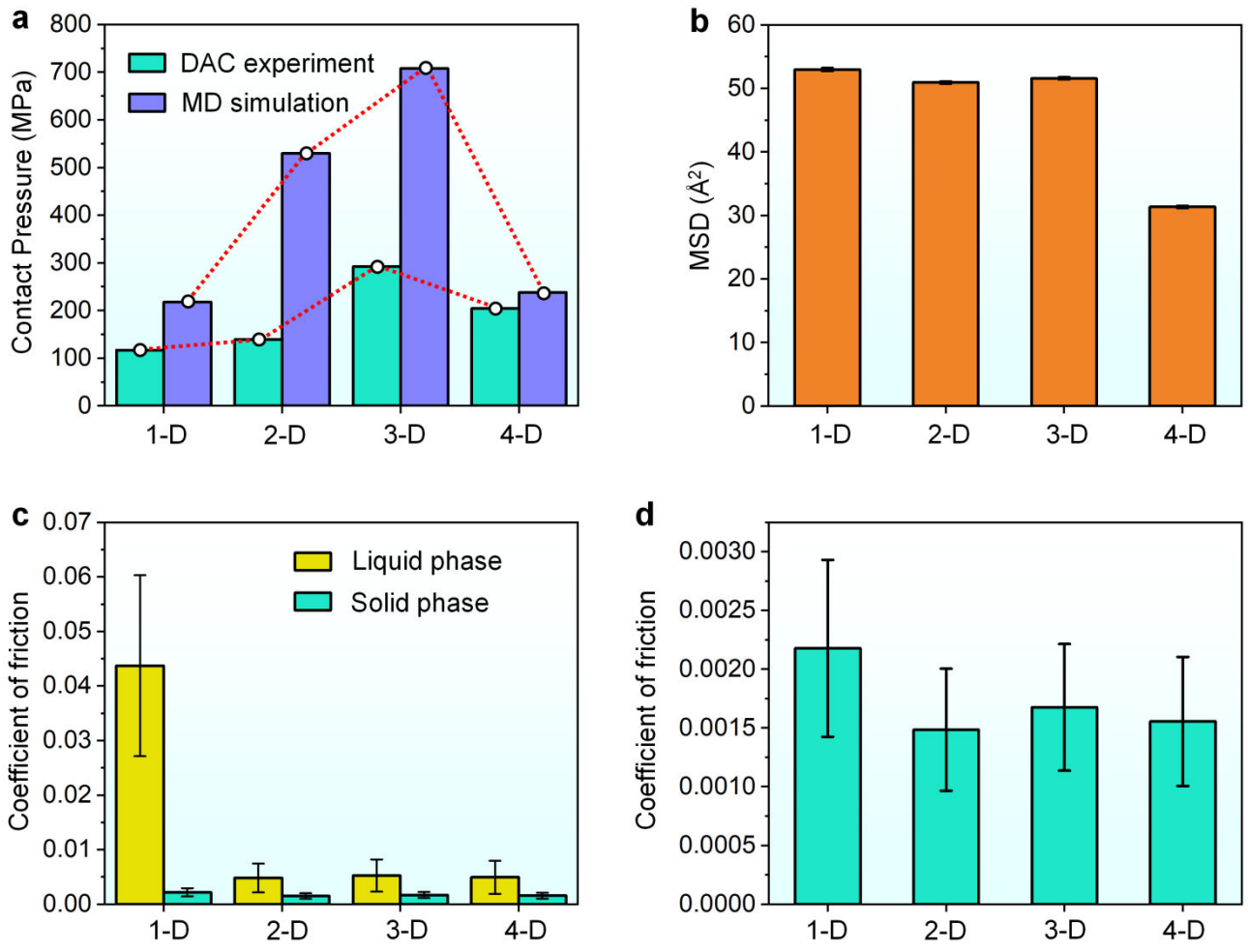

Fig. S23 | Characteristic parameters obtained from MD simulations of alkanol molecules with hydroxyl functional groups located at different positions along the carbon backbone. a Critical contact pressures for the phase transition of alkanol molecules with hydroxyl groups bonded at different positions along the carbon backbone, as determined by DAC experiments and MD simulations. Both DAC experiments and MD simulations revealed that when the hydroxyl group was bonded to the first three carbon atoms (1-D, 2-D, and 3-D), the critical contact pressure for the phase transition increased as the hydroxyl group was positioned closer to the center of the carbon backbone. However, when the hydroxyl group is bonded to the fourth carbon atom (4-D), the critical phase transition pressure no longer follows this trend, which may be related to the differences in the hydrogen-bond density. **b** Stable values of the MSD parameters after the phase transition for alkanol molecules with hydroxyl groups bonded at different positions along the carbon backbone. The data in (**b**) were obtained by averaging the values of the MSD parameters over the final 200 ps of the MD simulations. **c** Average COF of different alkanol molecules before (liquid phase) and after (solid phase) the phase transition. The average COF in the liquid phase was calculated over the first 50 ps of the MD simulations, whereas the average COF in the solid phase was calculated over the final 400 ps of the simulations. **d** Enlarged view of the average COF for alkanol molecules in the solid phase that exhibited in (**c**).

Supporting Movie Captions

Supplementary Movie 1:
Pressure induced reversible liquid-solid phase transition behavior of 1-dodecanol

Supplementary Movie 2:
Pressure induced reversible liquid-solid phase transition behavior of 1-undecanol

Supplementary Movie 3:
Pressure induced reversible liquid-solid phase transition behavior of 1-decanol

Supplementary Movie 4:
Pressure induced reversible liquid-solid phase transition behavior of 1-nonanol

Supplementary Movie 5:
Top view of the molecules migration process in the MD simulation of 1-dodecanol

Supplementary Movie 6:
Top view of the molecules migration process in the MD simulation of 1-undecanol

Supplementary Movie 7:
Top view of the molecules migration process in the MD simulation of 1-decanol

Supplementary Movie 8:
Top view of the molecules migration process in the MD simulation of 1-nonanol

Supplementary Movie 9:
Front view of the molecules migration process in the MD simulation of 1-dodecanol

Supplementary Movie 10:
Front view of the molecules migration process in the MD simulation of 1-undecanol

Supplementary Movie 11:
Front view of the molecules migration process in the MD simulation of 1-decanol

Supplementary Movie 12:
Front view of the molecules migration process in the MD simulation of 1-nonanol

Supplementary Movie 13:
Front view of the molecules migration of 1-dodecanol under different sliding velocities

Supplementary Movie 14:
Top view of the molecules migration of 1-dodecanol under different sliding velocities

Supplementary Movie 15:
Top view of the MD simulation of 2-dodecanol, 3-dodecanol, and 4-dodecanol

Supplementary Movie 16:
Front view of the MD simulation of 2-dodecanol, 3-dodecanol, and 4-dodecanol